ORIGINAL ARTICLE

^{1}H NMR-based metabolomic analysis of triptolide-induced toxicity in liver-specific cytochrome P450 reductase knockout mice

Xia Liu · Xiang Xue · Likun Gong · Xinming Qi · Yuanfeng Wu · Guozhen Xing · Yang Luan · Ying Xiao · Xiongfei Wu · Yan Li · Min Chen · Lingling Miao · Jun Yao · Jun Gu · Donghai Lin · Jin Ren

Abstract Triptolide (TL) is an active component of Tripterygium wilfordii Hook. F which is used to treat autoimmune and inflammatory disease. However, a high incidence of adverse effects is often observed in clinic. Previously we have demonstrated that cytochrome P450s (CYPs) are involved in the metabolism of TL and low activity of hepatic P450 reductase aggravates TL-induced toxicity. However, the underlying mechanisms of TL-induced toxicity mediated by hepatic CYPs have not been well delineated. Here, an integrated ^{1}H NMR-based metabolomic analysis was performed to evaluate the global biochemical alteration in the liver-specific cytochrome P450 reductase (CPR) knockout (KO) mice and wild-type (WT) counterparts with a same dose of TL (0.5 mg/kg) administration. Dramatically different metabolic profiles indicated more severe hepatotoxicity and nephrotoxicity induced by TL in KO mice than in WT mice, which were confirmed by serum biochemistry and histopathological examination. Furthermore, the results from both multivariate statistical analysis and system statistical metabolic correlation analysis indicated that the significantly changed endogenous metabolites were primarily involved in oxidative stress, energy metabolism, amino acid metabolism, gut microflora metabolism, and choline metabolism. Our results reveal the molecular mechanisms of TL-induced toxicity in the condition of hepatic CYP inactivation. As CYP inactivation and/or inhibition are usually caused by genetic polymorphism and/or drug–drug interactions, personalized prescription according to enzyme activity of CYPs and metabolic profiling could be used to maximize therapeutic efficacy and avoid or reduce TL-induced toxicity clinically.

Keywords Metabolomics · Triptolide · Toxicity · Cytochrome P450 · Hepatotoxicity

Xia Liu and Xiang Xue contribute equally to this work.

X. Liu
Biomolecular NMR Laboratory, Shanghai Institute of Materia Medica, Chinese Academy of Sciences, Shanghai, China

X. Xue · L. Gong · X. Qi · Y. Wu · G. Xing · Y. Luan ·
Y. Xiao · X. Wu · Y. Li · M. Chen · L. Miao · J. Yao ·
J. Ren (✉)
Center for Drug Safety Evaluation and Research, State Key Laboratory of Drug Research, Shanghai Institute of Materia Medica, Chinese Academy of Sciences, Shanghai, China
e-mail: jren@mail.shcnc.ac.cn

J. Gu
Wadsworth Center, New York State Department of Health, and School of Public Health, State University of New York at Albany, Albany, NY, USA

D. Lin (✉)
The Key Laboratory for Chemical Biology of Fujian Province, College of Chemistry and Chemical Engineering, Xiamen University, Xiamen, China
e-mail: dhlin@mail.shcnc.ac.cn

1 Introduction

Triptolide (TL) is a key biologically active component purified from Tripterygium wilfordii Hook. F (TWHF). It has many effective medicinal values including efficacies for the treatment of autoimmune and inflammatory diseases (Lin et al. 2007). However, its clinical use is limited by a narrow therapeutic window and high toxicity on digestive, urogenital, circulatory and reproductive systems, as well as

bone marrow (Mei et al. 2005; Ni et al. 2008). Previous work indicated that some crucial enzymes involved in the metabolism of TL could impact its toxicity (Li et al. 2008). In vitro studies demonstrated that two enzymes, CYP3A4 and CYP2C19, were involved in the conversion of TL into mono-hydroxylated metabolites (Li et al. 2008). High active hepatic CYP3A levels induced by dexamethasone treatment significantly increased the level of one mono-hydroxylated metabolite of TL and decreased its hepatotoxicity in rats (Ye et al. 2010). We have also demonstrated that inactivation of hepatic P450s abolishes the ability in metabolism of TL in the liver, subsequently resulting in an increase in bioavailability and toxicity of TL in vivo (Xue et al. 2011). However, the responsive changes of endogenous metabolites in vivo as a mechanism for TL-induced toxicity mediated by hepatic CYPs remain unclear.

As a potent approach for investigating drug toxicity, metabolomic analysis can provide a holistic view at the molecular level and offer an opportunity to better understanding mechanisms underlying toxicity (Boudonck et al. 2009; Powers 2009; Wei et al. 2009). Previous metabolomic studies have also indicated that TL perturbs metabolic pathways, including energy metabolism, amino acid metabolism, choline metabolism, and gut microflora metabolism (Chen et al. 2008; Liu et al. 2008; Xia et al. 2009). However, those studies were usually limited to urinary metabolic analysis and TL-induced toxicity with normal activity of drug metabolizing enzymes. Multi-organ metabolic profiling is required for addressing TL-induced toxicity affected by low activity of drug metabolizing enzymes and also for elucidating detailed molecular mechanisms.

Low activities of drug metabolic enzymes induced by genetic polymorphism usually lead to reduce efficacy and/or increase unfavorable adverse effects of drugs. In this present work, we performed an integrated ^{1}H NMR-based metabolomic analysis for liver aqueous extracts, kidney aqueous extracts, sera, and urine to assess the effects of hepatic CYP inactivation on TL-induced toxicity, which also offered a comprehensive understanding of the underlying modulation mechanisms. We adopted a well-developed model, the liver-specific cytochrome P450 reductase (CPR) knockout (KO) mouse (Gu et al. 2003; Henderson et al. 2003), in which the *CPR* gene encoding for the sole electron donor for all microsomal CYPs was deleted specifically in the liver, resulting in a loss of hepatic CYP activity (about 95%). Our results demonstrate that hepatic CYP activity play critical roles in the manipulation of TL-induced toxicity, which is reflected by the disturbed metabolic networks involving in oxidative stress, energy metabolism, amino acid metabolism, choline metabolism, and intestinal microflora ecosystem. To our knowledge, this is the first time to delineate the CYP-mediated drug toxicity using metabolomic analysis.

2 Experimental

2.1 Chemicals

TL ($C_{20}H_{24}O_6$, 99% purity), a major component of diterpenoid triepoxide lactone in the Chinese traditional herb TWHF, was provided by Prof. Yuanchao Li (Kupchan et al. 1972) (Shanghai Institute of Materia Medica, Chinese Academy of Sciences, China).

2.2 Animal treatments

The CPR KO mouse model is a gift from Prof. Xinxin Ding (Wadsworth Center, Albany, NY, USA). Procedures for animal breeding and genotyping were reported previously (Xiao et al. 2008). KO mice and their WT littermates (56–70 days in age, 24–26 g in weight) were used in this work. Animal use protocols were approved by the Institutional Animal Care and Use Committee of Shanghai Institute of Materia Medica, Chinese Academy of Sciences, China (Approval ID: SIMM-AE-(M3)2008-092). All the animals were provided with a certified standard diet and tap water ad libitum during the experiments including urine collection period. TL was first dissolved in dimethyl sulfoxide (DMSO) to make a stock solution at 5 mg/ml and then diluted with physiological saline to a final concentration of 0.025 mg/ml. Mice were oral administrated either with 0.2 ml of triptolide at the final concentration per 10 g to achieve a dose of 0.5 mg/kg or with 0.5% DMSO in physiological saline as solvent control as described previously (Xue et al. 2011). The reason for choosing this dose is that after a single dose of triptolide by oral gavage at 0.5 mg/kg, we observed no death in WT mice, whereas all of KO mice were dead in 5 days (Xue et al. 2011).

Urine samples were collected at the interval of 12–24 h after administration in solid CO_2-cooled tubes containing 20 μl of 1% (w/v) sodium azide. Aliquots of urine ranging in volume from 200 to 500 μl were obtained from each mouse and stored at −80°C before NMR analysis. Unfortunately, as one of urine samples from the WL group was contaminated by feces, only five urine specimens were used for the metabolic analysis of the WL. At 24 h after TL treatment, mice were euthanized with CO_2 and blood was drawn from each mouse to prepare serum samples in duplicate for both serum biochemistry and metabolomics analysis. The right lobe of liver and the right kidney from each mouse were collected and snap-frozen in liquid nitrogen and subsequently stored at −80°C before NMR analysis. The left lobe of liver and the left kidney from each mouse were used for histological examination as described previously (Xue et al. 2011).

2.3 ^{1}H NMR experiments

Lyophilized aqueous liver and entire right kidney extracts were prepared using the methanol/chloroform/water system as reported (Beckonert et al. 2007). Before NMR acquisition, 600 µl of phosphate buffer (0.2 M Na_2HPO_4/0.2 M NaH_2PO_4, pH 7.4) was added into aqueous tissue extract powder. Aliquots of urine or sera (200 µl) were mixed with 400 µl of phosphate buffer to control pH in a narrow range. All the mixed samples were vortexed and then centrifuged at $12,000 \times g$ for 10 min at 4°C. The collected supernatants (500 µl) were transferred into 5 mm NMR tubes and then 50 µl of D_2O containing 2.26 mM sodium 3-(trimethylsilyl) [2, 2, 3, 3-D4] propionate (TSP) was added. D_2O was used for field frequency lock, and TSP provided the chemical shift reference (δ 0.00). All NMR spectra were recorded at 25°C on a Varian Unity INOVA 600 MHz spectrometer equipped with three RF channels and a triple resonance z-axis pulsed-field gradient probe.

Standard one-dimensional (1D) PRESAT spectra of aqueous tissue extracts were acquired using a single 90° pulse sequence with an irradiation on the water resonance during the relaxation delay (RD) of 4 s. The 90° pulse length was adjusted to about 10 µs. A total of 128 transients were collected into 32 k data points using a spectral width of 10 kHz, giving an acquisition time (ACQ) of 1.64 s.

Transverse relaxation-edited spectra of serum samples were recorded using the water-suppressed Carr-Purcell-Meiboom-Gill (CPMG) pulse sequence [RD-90°-(τ-180°-τ)n-ACQ] with water suppression. A fixed total spin–spin relaxation delay 2 nτ of 120 ms were used to attenuate broad NMR signals of slowly tumbling molecules with short T_2 relaxation times and to retain signals of low-molecular weight compounds. The spectral width was 20 ppm with an acquisition time per scan of 1.60 s, and a total of 128 transients were collected into 32 k data points for each spectrum.

Solvent-suppressed 1D NOESY spectra of urine samples were acquired using the pulse sequence [RD-90°-t_1-90°-t_m-90°-ACQ]. t_1 was 6.6 µs. Water suppression was achieved by irradiation of the water resonance during the recycle delay of 4 s and mixing time (t_m) of 120 ms. Other parameters were the same as those used for acquiring 1D CPMG spectra.

To confirm resonance assignments for 1D ^{1}H NMR spectra, 2D pulsed field gradient COrrelation SpectroscopY with presaturated water resonance (gCOSYpr), together with 2D homonuclear TOtal Correlation SpectroscopY with DIPSI spinlock and watergate (wgTOCSY) were acquired on selected samples. In 2D NMR experiments, 64 transients per increment and 256 increments were collected into 1,024 data points, with spectral width of 8 kHz in both dimensions.

2.4 Multivariate statistical analysis

To exploit the metabolic information embedded in the spectra, all 1D ^{1}H NMR spectra were multiplied by an exponential function of a 0.3 Hz line-broadening factor prior to Fourier transformation, manually phased, corrected for baseline distortion, and carefully aligned. The NMR spectra of urine and tissue extract samples were referenced to the methyl group of TSP at 0.00 ppm, while ^{1}H CPMG spectra of serum samples were referenced to the methyl group of taurine at 3.27 ppm. The spectral region of δ 9.50–0.50 was segmented into 3,000 bins of a 0.003 ppm width for serum CPMG spectra and urine NoesyPr1d spectra, and 9,000 bins of a 0.001 ppm width for PRESAT spectra of aqueous tissue extracts. NMR data processing was conducted using the software MestReNova Version 5.3.1 (Mestrelab Research S.L.). The integrals from the region of δ 5.20–4.60 were excluded to eliminate distorted baseline from imperfect water saturation in all spectra. The integrals of residual methanol (δ 3.34–3.38) and ethanol (δ 1.16–1.20) from the spectra of aqueous tissue extracts were removed as well. In addition, the region of δ 6.00–5.20 including the broad urea peak, δ 3.16–3.17 and δ 2.73–2.74 including the signals of DMSO and its metabolite, were also excluded from the urine data (those peaks are not obvious in CPMG spectra of serum samples). The integrals of δ 1.33–1.42 and δ 4.10–4.18 including the signals of lactate were removed in the serum spectra for lactate was the highest signal (Fig. S1C) which would have the largest variance (Wang et al. 2004) and influence the clustering of four groups in the PCA scores plot of the serum ^{1}H-NMR data.

The remaining integrals for each NMR spectra were normalized by sum of the spectral intensity to compensate for differences in sample concentration. Subsequently, the integral values were mean-centered for PCA and OPLS-DA by the SIMCA-P + 12.0 software package (Umetrics, Umeå, Sweden). The terms R2X(cum), R2Y(cum), and Q2(cum) were used to evaluate the quality of OPLS-DA models. The R2X(cum) and R2Y(cum) are the fraction of the sum of the squares of the entire X's and Y's explained by the model, respectively. Q2(cum) represents the cross-validated explained variation. The reliability of the model increases with R2Y(cum) and Q2(cum) approaching to 1 (Weljie et al. 2007). Due to small numbers of animals used in this work (KC: WC: KL: WL = 7: 5: 6: 6), the (n_{min} − 1)-round cross validation and permutation test (999 cycles) on the first predictive component were carried out to measure the robustness of the model. The OPLS-DA loading plots were used to identify metabolites that are responsible for the separation of samples (Cloarec et al. 2005). The correlation coefficients of the variables relative to the predictive component (t[1]) in the OPLS-DA model were also calculated in a java environment (the software environment was downloaded freely from the URLs:

The critical values were referred to the table of critical values of correlation coefficient according to the degrees of freedom (df) which were determined as $n_1 + n_2 - 2$ with n_1 and n_2 as the respective number of samples of the two groups in the OPLS-DA model. When $|r|$ is greater than the critical value of $P = 0.01$, the peak was marked with red color and the higher the correlation coefficient $|r|$, the deeper the red color; when $|r|$ is between the critical values of $P = 0.05$ and 0.01, the peak was marked by yellow color; when $|r|$ is less than the critical value of $P = 0.05$, the peak was marked by blue color.

2.5 Quantitative comparison of significant metabolites

The relative integrals of metabolites whose correlation coefficient absolute number ($|r|$) are larger than the critical value of $P = 0.05$ were used for comparison between groups. The average changes and standard error were calculated (Carrola et al. 2011).

2.6 System statistical metabolic correlation analysis

A system statistical metabolic correlation analysis was further applied to display the relationships between the relative integrals of spectral peaks in a certain biological profile, as described previously (Lanza et al. 2010; Sands et al. 2009; Waldram et al. 2009). The integral of each verified metabolite of a compartment from the same mice within KL, KC, WL and WC groups was used as the variables for the metabolic correlation analysis. Six samples in KL and KC groups and five in WL and WC groups were used for this analysis. Pearson's correlation coefficients were calculated among those variations in the java environment mentioned above. A score plot was used to display the correlation matrices by the software of Spotfire decisionsite Version 9.1.1 (Spotfire AB, USA). An absolute value of correlation coefficient $|r|$ either larger than $0.811\,(P = 0.05)/0.878\,(P = 0.05)$ or larger than $0.917\,(P = 0.01)/0.959\,(P = 0.01)$ indicates a statistically or dramatically significant relationship between two metabolites. Significant positive correlations were marked with gradient red colors in the pixel map, significant negative correlations were indicated with gradient blue colors and insignificant correlations were shown as yellow color.

3 Results

## 3.1 Metabolic profiles of aqueous liver extracts, aqueous kidney extracts, sera, and urine

Typical ^{1}H NMR spectra of these samples obtained from a KL mouse are illustrated in Fig. S1. The metabolite

resonances were assigned according to literatures (Ding et al. 2009; Fan and Lane 2008; Tang et al. 2004), chemical shifts, proton–proton coupling constants and results from 2D NMR spectra (Table S1, Chemical shift and multiplicity). NMR spectra of aqueous tissue extracts and body fluids were dominated by the signals from amino acids, carboxylic acids, membrane components. The analysis of such complicated spectra could be greatly facilitated by multivariate statistical analysis, such as Principal Component Analysis (PCA) and Orthogonal Projection to Latent Structures Discriminant Analysis (OPLS-DA). Thus, mean-centered ^{1}H NMR variables were imported into the SIMCA-P + 12.0 software package (Umetrics, Umeå, Sweden) for PCA and OPLS-DA.

To obtain a comprehensive comparison of metabolic profiles among groups, scores plots of PCA with the first two principal components (t[1], t[2]) were employed (Fig. 1). The common feature of these PCA models is that the KL is metabolically differentiated from other three groups basically by the first principal component. The groups of WL, WC and KC display separations with partial overlap in the scores plots of aqueous liver extracts, sera and urine. It is worthwhile to note that WL, WC, and KC samples overlap with each other in the scores plot of aqueous kidney extracts (Fig. 1b), indicative of similar metabolic profiles of these three groups. To assess the variations between groups, OPLS-DA with one predictive (tp[1]) and one orthogonal component (to[1]) would like to be utilized.

To identify metabolites significantly contributing to the classification of metabolic profiles, sixteen pairwise OPLS-DA models (four in each compartment: aqueous liver extracts, aqueous kidney extracts, sera and urine) were constructed (Figs. S2–S5). The OPLS-DA models show distinct separations between the KL and the KC, the KL and the WL, the WL and the WC, the KC and the WC (Figs. S2–S5). The parameters of R2X(cum), R2Y(cum), and Q2(cum) were used to evaluate the robustness and reliability of the OPLS-DA models (Table S2). The permutation tests (Figs. S2–S5) strongly indicate that twelve of the OPLS-DA models are valid, shown by the observations that the Q2 regression line has a negative intercept and Q2 values to the left are lower than the original point to the right. However, it should be noted that for aqueous kidney extracts, both Q2 (cum) (0.277) from the model of KC versus WC and R2X(cum) (0.420) from the model of WL versus WC are relatively low. Their respective permutation tests are also indicative of overfit shown as some Q2 values to the left are higher than the original point to the right (Fig. S3C, D). Additionally, the OPLS-DA models of WL versus WC and KC versus WC (Fig. S5C, D) from urine NMR data were also not valid.

Fig. 1 PCA scores plots of ^{1}H NMR data of aqueous liver extracts (**a**), aqueous kidney extracts (**b**), sera (**c**), and urine (**d**). Models include KO control (KC, *triangle*), WT control (WC, *open triangle*), 0.5 mg/kg TL-treated KO (KL, *box*) mice, and 0.5 mg/kg TL-treated WT (WL, *square*) mice. Model parameters are shown as follows: **a** R2X(cum) = 0.801, Q2 (cum) = 0.733; **b** R2X(cum) = 0.740, Q2 (cum) = 0.599; **c** R2X(cum) = 0.694, Q2 (cum) = 0.582; and **d** R2X(cum) = 0.824, Q2 (cum) = 0.730
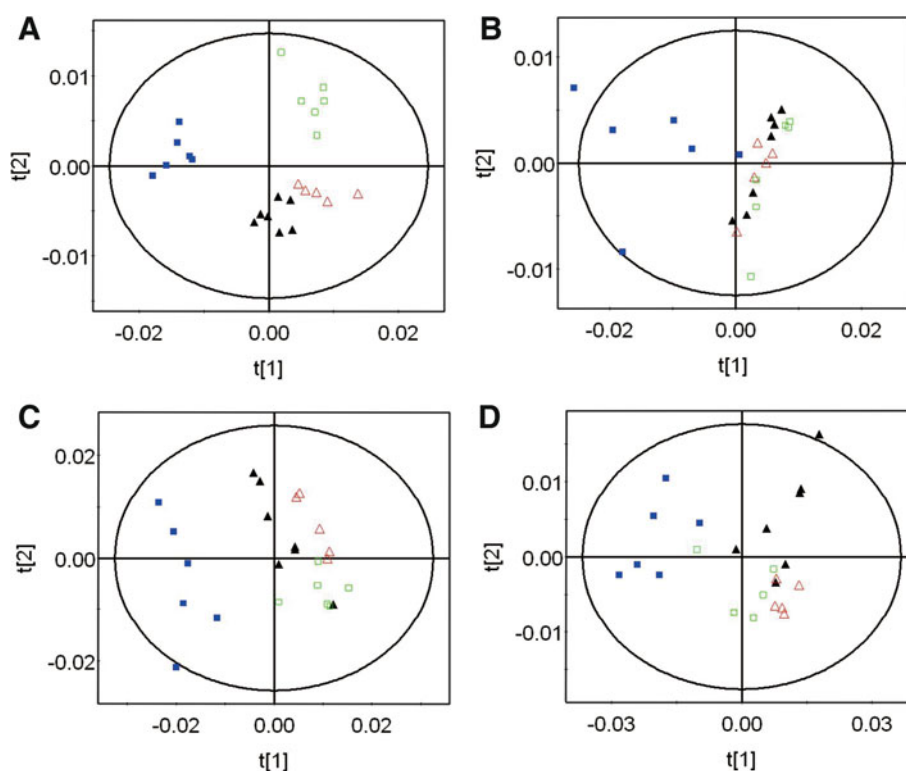
In order to identify the significant metabolites accountable for the separation, we established coefficient loading plots of the OPLS-DA models with critical values of coefficient number corresponding to $P = 0.05$ and 0.01. The coefficient loading plots of KL versus KC are shown for aqueous liver extracts (Fig. 2a), aqueous kidney extracts (Fig. 2b), sera (Fig. 2c), and urine (Fig. 2d), revealing a fluctuation of metabolite composition between groups. Furthermore, these altered metabolites are connected to different pathways and key enzymes referring to the Kyoto Encyclopedia of Genes and Genomes (KEGG) Database (Okuda et al. 2008) and the Human Metabolome Database (HMDB) (Wishart et al. 2007).

Additionally, we calculated the relative integrals of metabolites for discrimination based on the ^{1}H NMR variables and the average changes between groups which are shown in Tables 1, 2 and Tables S3, S4. The numbers of discriminated metabolites observed in the models of the KL versus KC and the KL versus WL are larger than those in the models of the WL versus WC and the KC versus WC.

3.2 System statistical metabolic correlation analysis

To explore latent relationships among metabolites and the interrupted metabolic pathways in the treatment groups, we calculated Pearson's correlation coefficients of the relative integrals of metabolites (Figs. S6–S9). Both the left-top KL/WL group and the right-bottom KC/WC group displayed different correlation patterns.

Several disordered metabolic networks in the dosed groups were shown in the correlation plot of metabolites in aqueous liver extracts (Fig. S6). (1) Amino acid metabolism was interrupted in KL and WL groups in various degrees. Branched chain amino acids (BCAAs, including Ile, Val, Leu) had positive correlations with lysine, glutamine, glutamate, aspartate, and glycine in the WC, which were disappeared in the KL and WL group. (2) Energy metabolism was disturbed in dosed groups. Malate was correlated negatively with lactate, positively with isoleucine, leucine, valine, glutamine, glutamate, succinate, and allantoin in the WC. Fumarate was correlated positively with leucine in the WC. However, the correlations of malate and isoleucine, fumarate and leucine were negatively in WL mice, and malate was negatively associated with valine in the KL. (3) The synthesis of glutathione (GSH) was disturbed in the KL. GSH positively correlated with cysteine and glycine in the WL. However, GSH exhibited negative correlation with cysteine in the KL. The above-mentioned metabolic disordered pathways were also observed in the correlation plots of metabolites in kidney, serum and urine (Figs. S6–S9).

4 Discussion

In the present work, the metabolic profiles of four groups revealed by PCA indicate that TL treatment could induce more severe metabolic alteration in KL mice than those in WL mice, verifying by that KL mice presented more severe
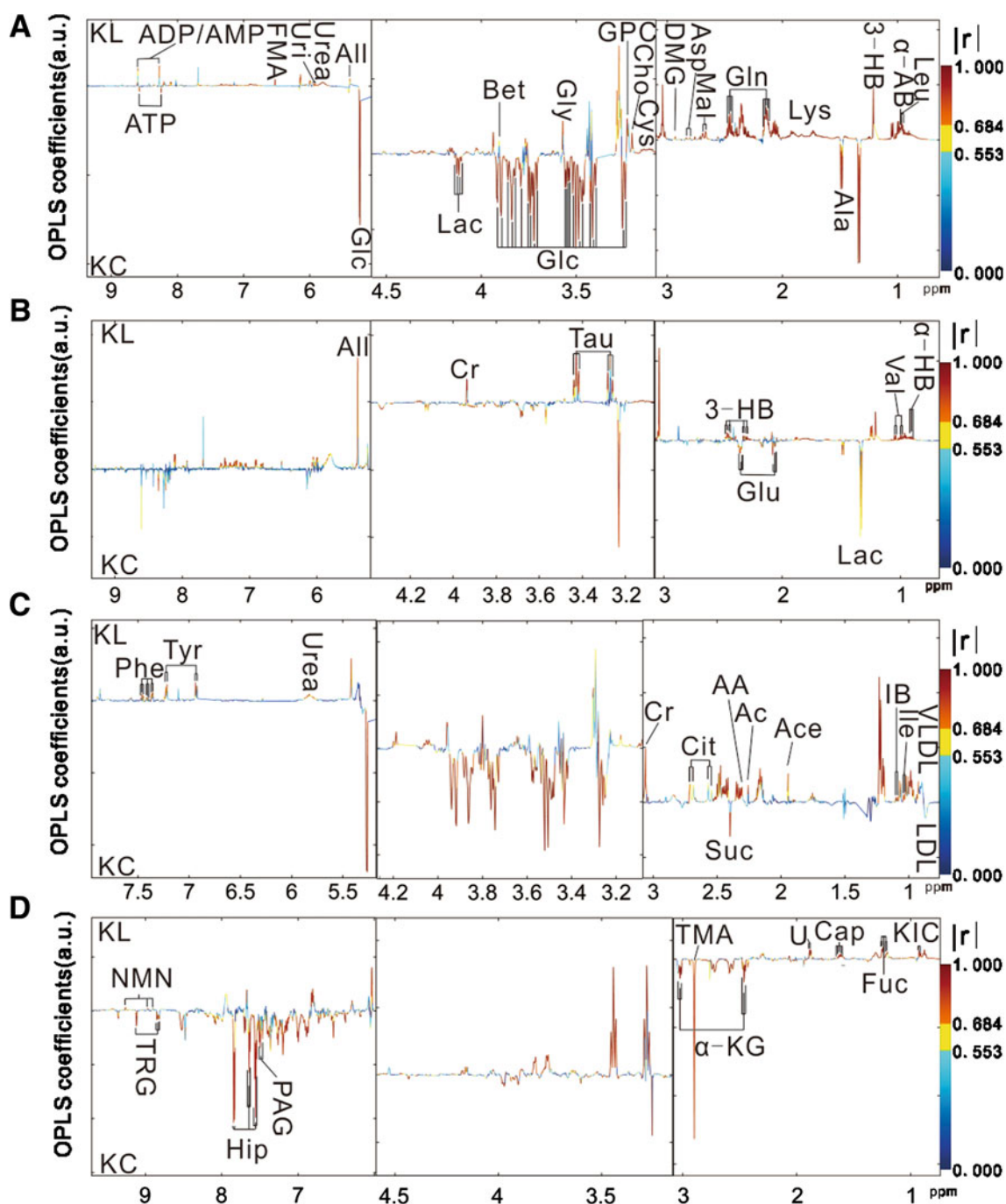
Fig. 2 OPLS-DA loading plots of ^{1}H NMR data from KL and KC groups of **a** Aqueous liver extracts, **b** aqueous kidney extracts, **c** sera, and **d** urine samples. The abbreviations of metabolites are denoted in Table S1

liver and kidney lesions than WL mice determined by serum biochemistry and histological examination (Tables S5, S6). The results from both OPLS-DA and system statistical metabolic correlation analysis probe the systemic disturbances in the metabolic profiles, including many biomarkers of hepatotoxicity and nephrotoxicity, and metabolites involving in oxidation stress, energy metabolism, amino acid metabolism, intestinal bacteria-related

metabolism, and choline metabolism, reflecting the molecular mechanisms of TL-induced toxicity by the intervention of low CYP activity (Fig. 3).

4.1 Biomarkers of hepatotoxicity

Both clinic chemistry and histopathology confirm TL-induced liver necrosis in KL mice, which is also supported

Table 1 The average changes of main metabolites contributing for discrimination of KL and KC in OPLS-DA models

Metabolites	δ ^{1}H(ppm)	% Average changes in liver	% Average changes in kidney	% Average changes in serum	% Average changes in urine
Cap	0.87	/	/	/	+98.9 ± 13.7
α-HB	0.90	+100.5 ± 31.5	+124.8 ± 7.4	/	/
KIC	0.92	/	/	/	+72.0 ± 11.2
Ile	1.01	+122.9 ± 35.3	+65.7 ± 5.2	+64.7 ± 24.4	/
Leu	0.96	+147.2 ± 25.8	+64.3 ± 5.2	+63.2 ± 15.1	/
α-AB	0.97	+274.6 ± 74.6	+122.7 ± 1.7	/	/
Val	1.05	+184.9 ± 44.5	+80.0 ± 1.0	+57.9 ± 25.3	/
IB	1.06	+96.0 ± 28.1	+90.3 ± 30.6	+109.4 ± 30.9	/
3-HB	1.21	+650 ± 91.8	+606.7 ± 150.5	+331.2 ± 51.3	/
Fuc	1.24	+115.4 ± 19.1	+597.5 ± 71.6	+175.6 ± 20.6	+93.7 ± 14.4
Lac	1.34	−58.1 ± 30.9	−40.0 ± 19.1	/	/
Ala	1.49	−55.7 ± 26.6	−28.6 ± 11.3	/	/
Lys	1.72	+126.7 ± 23.4	/	+39.4 ± 18.8	/
Ace	1.93	/	/	+40.5 ± 18.5	/
Ac	2.22	/	/	+103.8 ± 34.1	/
Glu	2.34	+220 ± 68.5	/	/	/
Suc	2.40	/	/	−53.7 ± 20.1	/
Gln	2.44	+66.2 ± 13.3	+74.3 ± 18.2	+105.0 ± 25.9	/
α-KG	2.45	/	/	/	−58.6 ± 30.1
Cit	2.55	/	/	/	−59.5 ± 26.4
MAL	2.68	+157.9 ± 23.8	+77.5 ± 18.2	/	/
Asp	2.82	+65.2 ± 26.1	/	/	/
TMA	2.86	/	/	/	−56.6 ± 22.5
DMG	2.93	+49.8 ± 13.4	/	/	−14.1 ± 2.5
Cr	3.95	+259.5 ± 119.5	+142.0 ± 25.9	+54.6 ± 13.7	/
Cys	3.11	+53.4 ± 7.5	/	/	/
Cho	3.21	+110.1 ± 30.0	/	/	−52.0 ± 26.3
PCho	3.22	+33.4 ± 23.2	/	/	/
GPC	3.23	+66.6 ± 8.6	−28.9 ± 11.5	/	/
Tau	3.27	+36.8 ± 12.0	+44.8 ± 11.1	+149.1 ± 58.5	+98.0 ± 23.0
Glc	3.84	−63.2 ± 35.3	/	−59.6 ± 31.7	/
Gly	3.57	+46.7 ± 15.9	−37.6 ± 10.9	/	/
All	5.38	+108.9 ± 53.7	+243.5 ± 23.4	+350.0 ± 178.7	/
Uri	5.92	+84.1 ± 32.2	/	/	/
Urea	5.80	+360.6 ± 118.3	+286.3 ± 55.6	+54.5 ± 5.0	/
FMA	6.52	+113.1 ± 21.7	/	/	−75.1 ± 37.9
tyr	7.18	/	+78.1 ± 8.9	+176.3 ± 47.2	−37.7 ± 15.5
Phe	7.34	/	+164.1 ± 8.8	+29.3 ± 15.2	/
PAG	7.34	/	/	/	−22.5 ± 4.7
Hip	7.82	/	/	/	−56.1 ± 21.6
ATP	8.58	−30.3 ± 16.9	/	/	/
ADP/AMP	8.60	+35.8 ± 14.8	/	/	/
For	8.46	/	/	+66.3 ± 33.3	/
TRG	9.11	/	/	/	−62.5 ± 34.8
NMN	9.25	/	/	/	+142.6 ± 40.5
U	1.88	/	+	/	+

Cap caprate, *a-HB* a-hydroxybutyrate, *KIC* α-ketoisocaproate, *Ile* isoleucine, *Leu* leucine, *α-AB* α-aminobutyrate, *Val* valine, *IB* isobutyrate, *3-HB* 3-hydroxybutyrate, *Fuc* fucose, *Lac* lactate, *Ala* alanine, *Lys* lysine, *Ace* acetate, *Ac* acetone, *Glu* glutamate, *Suc* succinate, *Gln* glutamine, *α-KG* α-ketoglutarate, *Cit* citrate, *MAL* malate, *Asp* aspartate, *DMG* N,N-dimethylglycine, *Cr* creatine, *Cys* cysteine, *Cho* choline, *PCho* O-phosphocholine, *GPC* sn-glycerol-3-phosphocholine, *Tau* taurine, *Glc* glucose, *Gly* glycine, *All* allantoin, *Uri* uridine, *FMA* fumarate, *Tyr* tyrosine, *Phe* phenylalanine, *PAG* phenylacetylglycine, *Hip* hippurate, *ATP* adenosine-triphosphate, *ADP/AMP* adenosine-diphosphate/adenosine-monophosphate, *For* formate, *TRG* trigonelline, *NMN* N1-methyl- nicotinamide, *U* an undetermined metabolite. "+" means an increase. "−" means a decrease. "/" means no significant change

by alterations of metabolic profiles of aqueous liver extracts, sera, and urine. In liver injury mouse models established by either carbon tetrachloride (CCl₄) (Robertson et al. 2000; Waterfield et al. 1991) or alpha-naphthyl-iso-thiocyanate (ANIT) (Azmi et al. 2005), the significant high level of taurine is a common feature. The elevation of taurine was detected in the liver, kidney, serum and urine of KL group, which might result from four factors: (1) leakage from damaged hepatocytes, (2) reduced reabsorption of taurine by the β-amino acid uptake system of the kidney due to renal damage (Waterfield et al. 1993), (3) perturbation of sulfur amino acid metabolism, and metabolic disturbance of GSH, (4) reduction in food intake results in decreased synthesis of taurocholic acid in bile.

Table 2 The average changes of main metabolites contributing for discrimination of WL and WC in OPLS-DA models

Metabolites	δ ^{1}H(ppm)	% average changes in liver	% average changes in kidney	% average changes in serum	% average changes in urine
Lipid	0.93	/	/	–	/
Leu	0.96	/	/	+56.7 ± 15.4	/
Ile	1.01	/	/	+77.9 ± 19.0	/
Val	1.05	/	/	+76.2 ± 24.0	/
IB	1.06	/	/	+75.9 ± 19.0	/
Lac	1.34	/	−21.4 ± 3.3	/	/
Lys	1.72	/	/	+54.9 ± 9.6	/
Ace	1.93	/	/	+45.7 ± 14.1	/
Ac	2.22	/	/	+41.0 ± 17.7	/
Suc	2.40	/	/	+14.4 ± 7.7	/
Gln	2.44	/	/	+81.1 ± 20.1	/
DMA	2.72	/	/	/	−24.8 ± 4.8
Asp	2.82	+37.9 ± 28.3	/	/	/
TMA	2.86	/	/	/	−17.4 ± 4.4
Cr	3.95	/	/	+41.5 ± 7.8	/
PCho	3.22	+43.7 ± 38.6	/	/	/
GPC	3.23	/	+12.3 ± 4.5	/	/
Tau	3.27	/	/	+47.6 ± 16.3	+84.4 + 41.1
Glc	3.84	−21.7 ± 5.8	/	−59.6 ± 31.7	/
Bet	3.90	+53.8 ± 11.1			/
Urea	5.80	+35.2 ± 13.5	+43.5 ± 37.6	+60.8 ± 18.2	/
tyr	7.18	/	+72.6 ± 17.8	+278.7 ± 99.9	/
Phe	7.34	/	/	+47.8 ± 22.6	/
For	8.46	+66.3 ± 33.3	/	/	/

Leu leucine, *Ile* isoleucine, *Val* valine, *IB* isobutyrate, *Lac* lactate, *Ala* alanine, *Lys* lysine, *Ace* acetate, *Ac* acetone, *Suc* succinate, *Gln* glutamine, *Cit* citrate, *DMA* N,N-dimethylamine, *Asp* aspartate, *TMA* trimethylamine, *Cr* creatine, *PCho* O-phosphocholine, *GPC* sn-glycerol-3-phosphocholine, *Tau* taurine, *Glc* glucose, *Bet* betaine, *Tyr* tyrosine, *Phe* phenylalanine, *For* formate. "+" means an increase. "−" means a decrease. "/" means no significant change

Necrotic hepatocytes and kidney damage might account for the first and second factors. Increased levels of cysteine in the liver and kidney might result from proteolysis and metabolic disorder of GSH. In addition, cysteine could also synthesize taurine by sequential actions of cysteine dioxygenase (Stipanuk 2004). TL-induced toxicity might induce loss of appetite in the mouse and decrease lipid uptake, leading to reduction of the synthesis of taurocholic acid, which might also contribute to the accumulation of taurine (Kay and Entenman 1961). The augmented level of taurine in the serum and urine of the WL compared with WC was less than that of the KL versus KC, which suggested that TL induced less severe liver injury in WT mice than in KO mice.

GPC is a constituent of the cell membrane, and its increase in the liver of KL mice might be caused by TL-induced necrotic hepatocytes and degradation of membranes including the mitochondrial membrane (Griffin et al. 2001). Choline is a degraded product of GPC, which can account for the observation that elevated GPC was positively correlated with increased choline in aqueous liver extracts of KL mice (Fig. S6A). However, these two metabolites were not obviously changed in aqueous liver extracts of WL mice, which were evidenced by no pertinent hepatocyte necrosis observed in the histological examination of WL mice.

Fucose was dramatically increased in KL mice compared with that of KC mice. Fucose is a common component in the synthesis of glycoproteins and glycolipids in Golgi apparatus (Sturgess et al. 1973). In patience with liver disease (Yamauchi et al. 1993), cirrhosis (Sakai et al. 1990) and drug-induced toxicity (Prince and Kannan 2006), the terminal glycosylation of glycoproteins in the Golgi apparatus is impaired and then free fucose will be accumulated. Therefore, fucose may serve as a biomarker for liver injury.

Therefore, high taurine, GPC, and fucose may serve as the potential biomarkers of hepatotoxicity. Fucose was negatively related with the decreased GPC in the serum of

KL and WL mice, suggesting the metabolic disorder of fucose might be induced by the defective membranes.

4.2 Biomarkers of nephrotoxicity

The elevated serum levels of BUN and CRE, kidney proximal tubular dilation (Fig. S10), together with significant alteration in metabolic profile of aqueous kidney extracts were observed in KL mice, whereas no obviously change was detected in WL mice, suggesting a direct outcome of TL-induced toxicity in the kidney regulated by hepatic CYPs. CRE, as a breakdown product of phosphocreatine in muscle and a dehydration product of creatine in the liver, kidney, muscle and pancreas (Milhorat 1953), is usually increased in serum during acute or chronic kidney injury (Ferguson et al. 2008; Kutlu et al. 2007). The accumulation of creatine in the liver, kidney, and serum of KL mice might be the result of the excess synthesis of creatine in tissue.

BCAAs are produced in the liver and degraded in the kidney, skeletal muscle, and other tissues (Harper 1989). Compared with those in KC and WL groups, the enhanced levels of BCAAs in the KL might result from the inhibition of the branched-chain α-keto acid dehydrogenase complex by TL-induced toxicity, such as renal dysfunction.

GPC, as an osmolyte in renal medullary cells (Kwon et al. 1995; Zablocki et al. 1991), decreased in the kidney of KL compared with KC mice (Table S3), implying severe disturbance of osmotic pressure in the kidney of KL mice.

The significantly increased amount of N1-methylnicotinamide in urine of the KL is indicative of transporter dysfunction in the renal proximal tubule (Musfeld et al. 2001), suggesting the damage of the proximal tubules as observed in histological examination of KL kidney. Furthermore, the decreased glycine in the kidney of the KL is possibly related to damage in the S3 region of the proximal tubules (Bairaktari et al. 2002).

Fucose is found in the proximal tubules of kidney (Hirano et al. 2005). In this study, we found the level of fucose in kidney was dramatically increased in KL compared to KC mice. This might suggest increased fucose in kidney was due to impaired proximal tubules.

In general, the accumulation of BUN, CRE, creatine, BCAA, N1-methylnicotinamide, fucose in kidney and body fluids combined with the depletion of glycine and GPC in kidney suggest the impairment of the kidney and the metabolites above-mentioned may be the biomarkers of nephrotoxicity.

4.3 Oxidative stress

The ascending levels of α-aminobutyrate and α-hydroxybutyrate in the liver and kidney of the KL might be
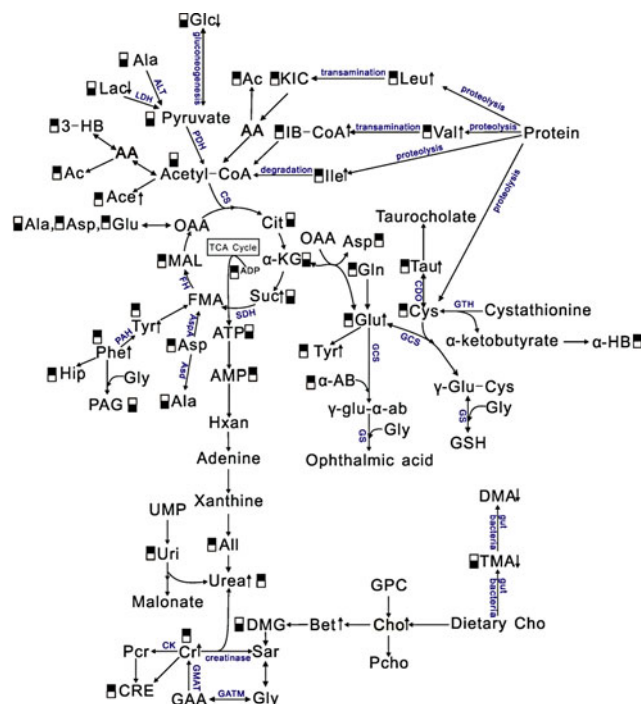

Fig. 3 Potential metabolic pathways disturbed by TL treatment. Metabolites marked by ■/■ means increased/decreased in KL mice as compared to KC mice. Metabolites with ↑/↓ means increased/decreased in WL mice relatively to WC mice. *Abbreviation*: *SDH*, succinate dehydrognase (EC: 1. 3. 5. 1); *FH*, fumarate hydratase (EC: 4. 2. 1. 2); *CS*, citrate synthase (EC: 2. 3. 3. 1); *ALT*, alanine transminase (EC: 2. 6. 1. 2); *AspA*, aspartate ammonia-lyase (EC: 4. 3. 1. 1); *ACH*, acetyl-CoA hydrolase (EC: 3. 1. 2. 1); *Asd*, aspartate 4-decarboxylase (EC: 4. 1. 1. 12); *LDH,* lactate dehydrogenases (EC: 1. 1. 1. 3, EC: 1. 1. 1. 27, EC: 1. 1. 1. 28, EC: 1. 1. 1. 4); *GCS,* c-glutamylcysteine synthetase (EC: 6. 3. 2. 2); *GS,* glutathione synthetase (EC: 6. 3. 2. 3); *CTH,* cystathionine gama-lyase (EC: 4. 4. 1. 1); *PAH,* phenylalanine-4-hydroxlase (EC: 1. 14. 16. 1); *CDO,* cysteine dioxygenase (EC: 1. 13. 11. 20); *GATM,* glycine amidinotransferase (EC: 2. 1. 4. 1); *GAMT,* guanidinoacetate N-methyltransferase (EC: 2. 1. 2. 2); *CK,* Creatine kinase (EC: 2. 7. 3. 2); Creatinase (EC: 3. 5. 3. 3); *Pcr,* Phosphocreatine; *CRE,* creatinine; *Arg,* arginine; *OAA*, oxaloacetate. The abbreviations of other metabolites are denoted in Table S1

predictors of oxidative damage. α-hydroxybutyrate is an organic acid converted from α-ketobutyrate, α-ketobutyrate is released when cystathionine is cleaved to cysteine by cystathionine gama-lyase, and then cysteine and glutamate are catalyzed by glutamate-cysteine ligase to synthesize γ-Glu-Cys which joins with glycine to form GSH by glutathione synthetase (Gall et al. 2010) (Fig. 3). In this work, GSH did not show significant change after TL treatment, possibly due to a relatively short examination time. However, the upregulated cysteine, α-hydroxybutyrate, and glutamate in the liver of the KL imply that the body sped up to synthesize GSH. In addition, α-aminobutyrate is a key precursor of ophthalmic acid that is a tripeptide analogue of GSH. Ophthalmic acid has a similar biosynthetic

route to GSH, except that its precursor is α-aminobutyrate instead of cysteine (Orlowski and Wilk 1978) (Fig. 3). Previous work has indicated that ophthalmic acid might be an oxidative stress biomarker (Soga et al. 2006).

Moreover, xanthine and uric acid could be oxidized to allantoin by various reactive oxygen species. Allantoin could be dramatically increased in plasma or sera of patients with oxidative stress situations such as chronic renal failure (Kand'ar and Zakova 2008), rheumatoid arthritis (Yardim-Akaydin et al. 2004), and chronic lung diseases (James et al. 2003), Thus, significantly elevated allantoin in the liver, kidney and sera of the KL also indicated severe oxidative damage induced by TL.

Overall, α-aminobutyrate, α-hydroxybutyrate, cysteine, and allantoin could serve as biomarkers of oxidative stress. However, those metabolites relative to oxidative stress didn't show significant change in WL mice compared with WC mice.

4.4 Energy metabolism disturbance

TCA cycle intermediates including citrate, α-ketoglutarate and fumarate were decreased in urine of KL group, accompanied by enhanced levels of malate and fumarate in aqueous liver extracts of the KL. This phenomenon might be attributed to the enhanced reabsorption of renal tubules to the intermediates of TCA cycle (Chen et al. 1998), which could lead to renal tubular acidosis (Hering-Smith et al. 2000).

Under normal biochemical circumstances, lactate can enter into gluconeogenesis via pyruvate to compensate for the loss of glucose (Solanky et al. 2003), thus the decreased levels of lactate in the liver and kidney of the KL imply a potential stimulation of gluconeogenesis. On the other hand, the consistent decreases of alanine and glucose in the KL (Table 1) imply TL-induced accelerating gluconeogenesis from alanine, which might account for the positive correlation between glucose and alanine in the liver of the KL (Fig. S6A). Depletion of carbohydrates may excite the elevation of ketone bodies (Massey et al. 1998). Thus, accompanied by the perturbation of energy metabolism, the augmented levels of ketone bodies were observed in serum after TL treatment (Table 1).

All above-mentioned abnormalities in energy metabolism were reflected by the depletion of ATP and the accumulation of ADP/AMP occurring in KL liver, suggesting the reduced synthesis and accelerated decomposition of ATP.

4.5 Amino acid metabolism disturbance

Elevated levels of amino acids including lysine, isoleucine, leucine, valine, glutamine, phenylalanine in serum, and tyrosine in KL and WL groups (Tables 1, 2) were indicative of the perturbation of protein biosynthesis and catabolism. Increases of these amino acids in the liver and kidney together with reduced serum total protein and albumin in the KL further confirm more severe occurrence of proteolysis than in the WL group.

4.6 Destroyed intestinal microflora and choline metabolism

As one of the short chain fatty acids, caproate is a product via microbial metabolism (Laerke et al. 2000; Macfarlane and Macfarlane 2003), its increase in urine of the KL might also be an indicator of altered microbial metabolism. The precursors of phenylacetylglycine and hippurate are also produced by gut bacteria (Delaney et al. 2004), thus the prominently decreased urinary phenylacetylglycine and hippurate observed herein in the KL imply potential damage to the intestinal environment.

Several strains of gut bacteria have been shown to decompose choline to trimethylamine (Wei et al. 2009). Decreased trimethylamine and N,N-dimethylglycine in KL urine show positive relationship respectively with phenylacetylglycine and hippurate (Fig. S7), suggesting the alteration of these metabolites may reflect the altered structure and activity of gut microbiota and choline metabolism.

Although the numbers of mice used in this work are relatively small (6, 6, 7, and 5 samples for the KL, WL, KC, and WC group, respectively), the metabolic profiles of KL group from PCA analysis are distinctly different from other three groups.

5 Conclusions

In summary, our results displayed the mechanisms of TL-induced toxicity by the intervention of hepatic CYPs. The perturbation of metabolic regulatory network revealed by ^{1}H NMR spectra combined with multivariate statistical analysis and system statistical metabolic correlation analysis may contribute to the molecular mechanisms of TL-induced toxicity mediated by low activity of CYPs. As shown in Fig. 3, in the KO group with lower CYP activity, 0.5 mg/kg dose of TL gravely interrupted energy metabolism, amino acid metabolism, intestinal microflora and choline metabolism and induced severe oxidative stress compared with WL mice. As CYP inactivation or inhibition are usually caused by genetic polymorphism and/or drug–drug interactions in clinic, personalized prescription according to the enzyme activity of CYPs and metabolic profiling could be employed to maximize therapeutic

efficacy and avoid TL-induced toxicity, especially when CYP inhibitors are clinically used together with TL.

References

Azmi, J., Griffin, J. L., Shore, R. F., Holmes, E., & Nicholson, J. K. (2005). Chemometric analysis of biofluids following toxicant induced hepatotoxicity: A metabonomic approach to distinguish the effects of 1-naphthylisothiocyanate from its products. *Xenobiotica, 35*(8), 839–852.

Bairaktari, E., Seferiadis, K., Liamis, G., Psihogios, N., Tsolas, O., & Elisaf, M. (2002). Rhabdomyolysis-related renal tubular damage studied by proton nuclear magnetic resonance spectroscopy of urine. *Clinical Chemistry, 48*(7), 1106–1109.

Beckonert, O., Keun, H. C., Ebbels, T. M., Bundy, J., Holmes, E., Lindon, J. C., et al. (2007). Metabolic profiling, metabolomic and metabonomic procedures for NMR spectroscopy of urine, plasma, serum and tissue extracts. *Nature Protocols, 2*(11), 2692–2703.

Boudonck, K. J., Rose, D. J., Karoly, E. D., Lee, D. P., Lawton, K. A., & Lapinskas, P. J. (2009). Metabolomics for early detection of drug-induced kidney injury: Review of the current status. *Bioanalysis, 1*(9), 1645–1663.

Carrola, J., Rocha, C. M., Barros, A. S., Gil, A. M., Goodfellow, B. J., Carreira, I. M., et al. (2011). Metabolic signatures of lung cancer in biofluids: NMR-based metabonomics of urine. *Journal of Proteome Research, 10*(1), 221–230.

Chen, M., Ni, Y., Duan, H., Qiu, Y., Guo, C., Jiao, Y., et al. (2008). Mass spectrometry-based metabolic profiling of rat urine associated with general toxicity induced by the multiglycoside of Tripterygium wilfordii Hook. f. *Chemical Research in Toxicology, 21*(2), 288–294.

Chen, X. Z., Shayakul, C., Berger, U. V., Tian, W., & Hediger, M. A. (1998). Characterization of a rat Na+-dicarboxylate cotransporter. *Journal of Biological Chemistry, 273*(33), 20972–20981.

Cloarec, O., Dumas, M. E., Trygg, J., Craig, A., Barton, R. H., Lindon, J. C., et al. (2005). Evaluation of the orthogonal projection on latent structure model limitations caused by chemical shift variability and improved visualization of biomarker changes in ^{1}H NMR spectroscopic metabonomic studies. *Analytical Chemistry, 77*(2), 517–526.

Delaney, J., Neville, W. A., Swain, A., Miles, A., Leonard, M. S., & Waterfield, C. J. (2004). Phenylacetylglycine, a putative biomarker of phospholipidosis: Its origins and relevance to phospholipid accumulation using amiodarone treated rats as a model. *Biomarkers, 9*(3), 271–290.

Ding, L., Hao, F., Shi, Z., Wang, Y., Zhang, H., Tang, H., et al. (2009). Systems biological responses to chronic perfluorododecanoic acid exposure by integrated metabonomic and transcriptomic studies. *Journal of Proteome Research, 8*(6), 2882–2891.

Fan, T. W. M., & Lane, A. N. (2008). Structure-based profiling of metabolites and isotopomers by NMR. *Progress in Nuclear Magnetic Resonance Spectroscopy, 52*(2–3), 69–117.

Ferguson, M. A., Vaidya, V. S., & Bonventre, J. V. (2008). Biomarkers of nephrotoxic acute kidney injury. *Toxicology, 245*(3), 182–193.

Gall, W. E., Beebe, K., Lawton, K. A., Adam, K. P., Mitchell, M. W., Nakhle, P. J., et al. (2010). Alpha-hydroxybutyrate is an early biomarker of insulin resistance and glucose intolerance in a nondiabetic population. *PLoS One, 5*(5), e10883.

Griffin, J. L., Mann, C. J., Scott, J., Shoulders, C. C., & Nicholson, J. K. (2001). Choline containing metabolites during cell transfection: An insight into magnetic resonance spectroscopy detectable changes. *FEBS Letters, 509*(2), 263–266.

Gu, J., Weng, Y., Zhang, Q. Y., Cui, H., Behr, M., Wu, L., et al. (2003). Liver-specific deletion of the NADPH-cytochrome P450 reductase gene: Impact on plasma cholesterol homeostasis and the function and regulation of microsomal cytochrome P450 and heme oxygenase. *Journal of Biological Chemistry, 278*(28), 25895–25901.

Harper, A. E. (1989). Thoughts on the role of branched-chain alpha-keto acid dehydrogenase complex in nitrogen metabolism. *Annals of the New York Academy of Sciences, 573*, 267–273.

Henderson, C. J., Otto, D. M., Carrie, D., Magnuson, M. A., McLaren, A. W., Rosewell, I., et al. (2003). Inactivation of the hepatic cytochrome P450 system by conditional deletion of hepatic cytochrome P450 reductase. *Journal of Biological Chemistry, 278*(15), 13480–13486.

Hering-Smith, K. S., Gambala, C. T., & Hamm, L. L. (2000). Citrate and succinate transport in proximal tubule cells. *American Journal of Physiology Renal Physiology, 278*(3), F492–F498.

James, T. J., Hughes, M. A., Cherry, G. W., & Taylor, R. P. (2003). Evidence of oxidative stress in chronic venous ulcers. *Wound Repair and Regeneration, 11*(3), 172–176.

Kand'ar, R., & Zakova, P. (2008). Allantoin as a marker of oxidative stress in human erythrocytes. *Clinical Chemistry and Laboratory Medicine, 46*(9), 1270–1274.

Kay, R. E., & Entenman, C. (1961). Stimulation of taurocholic acid synthesis and biliary excretion of lipids. *American Journal of Physiology, 200*, 855–859.

Kupchan, S. M., Court, W. A., Dailey, R. G., Jr., Gilmore, C. J., & Bryan, R. F. (1972). Triptolide and tripdiolide, novel antileukemic diterpenoid triepoxides from *Tripterygium wilfordii. Journal of the American Chemical Society, 94*(20), 7194–7195.

Kutlu, S., Colakoglu, N., Halifeoglu, I., Sandal, S., Seyran, A. D., Aydin, M., et al. (2007). Comparative evaluation of hepatotoxic and nephrotoxic effects of aroclors 1221 and 1254 in female rats. *Cell Biochemistry and Function, 25*(2), 167–172.

Kwon, E. D., Zablocki, K., Jung, K. Y., Peters, E. M., Garcia-Perez, A., & Burg, M. B. (1995). Osmoregulation of GPC:choline phosphodiesterase in MDCK cells: different effects of urea and NaCl. *American Journal of Physiology, 269*((1 Pt 1)), C35–C41.

Laerke, H. N., Jensen, B. B., & Hojsgaard, S. (2000). In vitro fermentation pattern of D-tagatose is affected by adaptation of the microbiota from the gastrointestinal tract of pigs. *Journal of Nutrition, 130*(7), 1772–1779.

Lanza, I. R., Zhang, S., Ward, L. E., Karakelides, H., Raftery, D., & Nair, K. S. (2010). Quantitative metabolomics by H-NMR and LC-MS/MS confirms altered metabolic pathways in diabetes. *PLoS One, 5*(5), e10538.

Li, W., Liu, Y., He, Y. Q., Zhang, J. W., Gao, Y., Ge, G. B., et al. (2008). Characterization of triptolide hydroxylation by cytochrome P450 in human and rat liver microsomes. *Xenobiotica, 38*(12), 1551–1565.

Lin, N., Liu, C. F., Xiao, C., Jia, H. W., Imada, K., Wu, H., et al. (2007). Triptolide, a diterpenoid triepoxide, suppresses

inflammation and cartilage destruction in collagen-induced arthritis mice. *Biochemical Pharmacology, 73*(1), 136–146.

Liu, M. X., Dong, J., Yang, Y. J., Yang, X. L., & Xu, H. B. (2008). Effect of poly(D, L-lactic acid) nanoparticles as triptolide carrier on abating rats renal toxicity by NMR-based metabolic analysis. *Journal of Nanoscience and Nanotechnology, 8*(7), 3493–3499.

Macfarlane, S., & Macfarlane, G. T. (2003). Regulation of short-chain fatty acid production. *Proceedings of the Nutrition Society, 62*(1), 67–72.

Massey, K. A., Blakeslee, C. H., & Pitkow, H. S. (1998). A review of physiological and metabolic effects of essential amino acids. *Amino Acids, 14*(4), 271–300.

Mei, Z., Li, X., Wu, Q., Hu, S., & Yang, X. (2005). The research on the anti-inflammatory activity and hepatotoxicity of triptolide-loaded solid lipid nanoparticle. *Pharmacological Research, 51*(4), 345–351.

Milhorat, A. T. (1953). Creatine and creatinine metabolism and diseases of the neuromuscular system. *Research Publications—Association for Research in Nervous and Mental Disease, 32*, 400–421.

Musfeld, C., Biollaz, J., Belaz, N., Kesselring, U. W., & Decosterd, L. A. (2001). Validation of an HPLC method for the determination of urinary and plasma levels of N1-methylnicotinamide, an endogenous marker of renal cationic transport and plasma flow. *Journal of Pharmaceutical and Biomedical Analysis, 24*(3), 391–404.

Ni, B., Jiang, Z. Z., Huang, X., Xu, F. G., Zhang, R., Zhang, Z. J., et al. (2008). Male reproductive toxicity and toxicokinetics of triptolide in rats. *Arzneimittel-Forschung-Drug Research, 58*(12), 673–680.

Okuda, S., Yamada, T., Hamajima, M., Itoh, M., Katayama, T., Bork, P., et al. (2008). KEGG Atlas mapping for global analysis of metabolic pathways. *Nucleic Acids Research, 36*(Web Server issue), W423–W426.

Orlowski, M., & Wilk, S. (1978). Synthesis of ophthalmic acid in liver and kidney in vivo. *Biochemical Journal, 170*(2), 415–419.

Powers, R. (2009). NMR metabolomics and drug discovery. *Magnetic Resonance in Chemistry, 47*(Suppl 1), S2–S11.

Prince, P. S. M., & Kannan, N. K. (2006). Protective effect of rutin on lipids, lipoproteins, lipid metabolizing enzymes and glycoproteins in streptozotocin-induced diabetic rats. *Journal of Pharmacy and Pharmacology, 58*(10), 1373–1383.

Robertson, D. G., Reily, M. D., Sigler, R. E., Wells, D. F., Paterson, D. A., & Braden, T. K. (2000). Metabonomics: Evaluation of nuclear magnetic resonance (NMR) and pattern recognition technology for rapid in vivo screening of liver and kidney toxicants. *Toxicological Sciences, 57*(2), 326–337.

Sakai, T., Yamamoto, K., Yokota, H., Hakozaki-Usui, K., Hino, F., & Kato, I. (1990). Rapid, simple enzymatic assay of free L-fucose in serum and urine, and its use as a marker for cancer, cirrhosis, and gastric ulcers. *Clinical Chemistry, 36*(3), 474–476.

Sands, C. J., Coen, M., Maher, A. D., Ebbels, T. M., Holmes, E., Lindon, J. C., et al. (2009). Statistical total correlation spectroscopy editing of 1H NMR spectra of biofluids: Application to drug metabolite profile identification and enhanced information recovery. *Analytical Chemistry, 81*(15), 6458–6466.

Soga, T., Baran, R., Suematsu, M., Ueno, Y., Ikeda, S., Sakurakawa, T., et al. (2006). Differential metabolomics reveals ophthalmic acid as an oxidative stress biomarker indicating hepatic glutathione consumption. *Journal of Biological Chemistry, 281*(24), 16768–16776.

Solanky, K. S., Bailey, N. J., Beckwith-Hall, B. M., Davis, A., Bingham, S., Holmes, E., et al. (2003). Application of biofluid ^{1}H nuclear magnetic resonance-based metabonomic techniques for the analysis of the biochemical effects of dietary isoflavones on human plasma profile. *Analytical Biochemistry, 323*(2), 197–204.

Stipanuk, M. H. (2004). Sulfur amino acid metabolism: Pathways for production and removal of homocysteine and cysteine. *Annual Review of Nutrition, 24*, 539–577.

Sturgess, J. M., Minaker, E., Mitranic, M. M., & Moscarello, M. A. (1973). The incorporation of L-fucose into glycoproteins in the Golgi apparatus of rat liver and in serum. *Biochimica et Biophysica Acta, 320*(1), 123–132.

Tang, H. R., Wang, Y. L., Nicholson, J. K., & Lindon, J. C. (2004). Use of relaxation-edited one-dimensional and two dimensional nuclear magnetic resonance spectroscopy to improve detection of small metabolites in blood plasma. *Analytical Biochemistry, 325*(2), 260–272.

Waldram, A., Holmes, E., Wang, Y., Rantalainen, M., Wilson, I. D., Tuohy, K. M., et al. (2009). Top-down systems biology modeling of host metabotype-microbiome associations in obese rodents. *Journal of Proteome Research, 8*(5), 2361–2375.

Wang, Y., Holmes, E., Nicholson, J. K., Cloarec, O., Chollet, J., Tanner, M., et al. (2004). Metabonomic investigations in mice infected with Schistosoma mansoni: an approach for biomarker identification. *Proceedings of the National Academy of Sciences of the United States of America, 101*(34), 12676–12681.

Waterfield, C. J., Turton, J. A., Scales, M. D., & Timbrell, J. A. (1991). Taurine, a possible urinary marker of liver damage: A study of taurine excretion in carbon tetrachloride-treated rats. *Archives of Toxicology, 65*(7), 548–555.

Waterfield, C. J., Turton, J. A., Scales, M. D. C., & Timbrell, J. A. (1993). Investigations into the effects of various hepatotoxic compounds on urinary and liver taurine levels in rats. *Archives of Toxicology, 67*(4), 244–254.

Wei, L., Liao, P., Wu, H., Li, X., Pei, F., Li, W., et al. (2009). Metabolic profiling studies on the toxicological effects of realgar in rats by (1)H NMR spectroscopy. *Toxicology and Applied Pharmacology, 234*(3), 314–325.

Weljie, A. M., Dowlatabadi, R., Miller, B. J., Vogel, H. J., & Jirik, F. R. (2007). An inflammatory arthritis-associated metabolite biomarker pattern revealed by ^{1}H NMR spectroscopy. *Journal of Proteome Research, 6*(9), 3456–3464.

Wishart, D. S., Tzur, D., Knox, C., Eisner, R., Guo, A. C., Young, N., et al. (2007). HMDB: the human metabolome database. *Nucleic Acids Research, 35*, D521–D526.

Xia, S. G., Liu, H. L., Zhu, H., Zhou, Z. M., Zhang, X., & Liu, M. L. (2009). NMR-based metabonomic study on rat's urinary metabolic response to dosage of triptolide. *Chinese Journal of Chemistry, 27*(4), 751–758.

Xiao, Y., Ge, M., Xue, X., Wang, C., Wang, H., Wu, X., et al. (2008). Hepatic cytochrome P450s metabolize aristolochic acid and reduce its kidney toxicity. *Kidney International, 73*(11), 1231–1239.

Xue, X., Gong, L., Qi, X., Wu, Y., Xing, G., Yao, J., et al. (2011). Knockout of hepatic P450 reductase aggravates triptolide-induced toxicity. *Toxicology Letters, 205*(1), 47–54.

Yamauchi, M., Kimura, K., Maezawa, Y., Ohata, M., Mizuhara, Y., Hirakawa, J., et al. (1993). Urinary level of L-fucose as a marker of alcoholic liver-disease. *Alcoholism-Clinical and Experimental Research, 17*(2), 268–271.

Yardim-Akaydin, S., Sepici, A., Ozkan, Y., Torun, M., Simsek, B., & Sepici, V. (2004). Oxidation of uric acid in rheumatoid arthritis: Is allantoin a marker of oxidative stress? *Free Radical Research, 38*(6), 623–628.

Ye, X., Li, W., Yan, Y., Mao, C., Cai, R., Xu, H., et al. (2010). Effects of cytochrome P4503A inducer dexamethasone on the metabolism and toxicity of triptolide in rat. *Toxicology Letters, 192*(2), 212–220.

Zablocki, K., Miller, S. P., Garcia-Perez, A., & Burg, M. B. (1991). Accumulation of glycerophosphocholine (GPC) by renal cells: Osmotic regulation of GPC:choline phosphodiesterase. *Proceedings of the National Academy of Sciences of the United States of America, 88*(17), 7820–7824.